IL NUOVO CIMENTO **38 C** (2015) 117
DOI 10.1393/ncc/i2015-15117-y

COLLOQUIA: LaThuile15

The Pierre Auger Observatory: Mass composition results and future plans

A. E. HERVÉ for the PIERRE AUGER COLLABORATION([2])([*])

([1]) *IKP, Karlsruhe Institute of Technology (KIT) - Postfach 3640 D-76021 Karlsruhe, Germany*
([2]) *Observatorio Pierre Auger - Av. San Martín Norte 304 5613 Malargüe, Argentina*

received 2 October 2015

Summary. — The Pierre Auger Observatory has been designed to study ultra-high energy cosmic rays. The study of their mass composition can help constrain models concerning their nature and origin. We discuss the different methods of deriving the mass composition of the primary cosmic rays. The methods use different parameters that describe various characteristics of the shower development. We will also discuss the prospects expected from an upgrade of the Pierre Auger Observatory.

1. – Introduction

The mass composition of ultra-high energy cosmic rays (UHECRs) is one of the main observables used to study the origin of these particles. The interpretation of features of the flux, such as the steepening observed around 4×10^{19} eV [1-3], and observed anisotropies [4, 5], relies on the assumed mass composition. The Pierre Auger Observatory [6, 7] is located in the Province of Mendoza, Argentina. It was completed in 2008 and covers an area of 3000 km^2. It is a hybrid detector, combining a surface detector array (SD) [8] and a fluorescence detector (FD) [9]. The SD is equipped with 1660 water-Cherenkov stations, arranged on a triangular grid with a 1500 m spacing (with some at a 750 m spacing), measuring the lateral distribution of particles at the ground. The FD consists of 27 optical telescopes which overlook the SD array. These are used to observe the longitudinal profile of showers by detecting fluorescence and Cherenkov light produced by the energy deposited by charged particles in the atmosphere. The overall uptime and efficiency of the SD is above 98%, while the FD can only operate on clear moonless nights and under favourable meteorological conditions leading to an uptime of 15%. The atmospheric depth where the longitudinal development of an air shower

([*]) Full author list: `http://www.auger.org/archive/authors_2015_02.html`

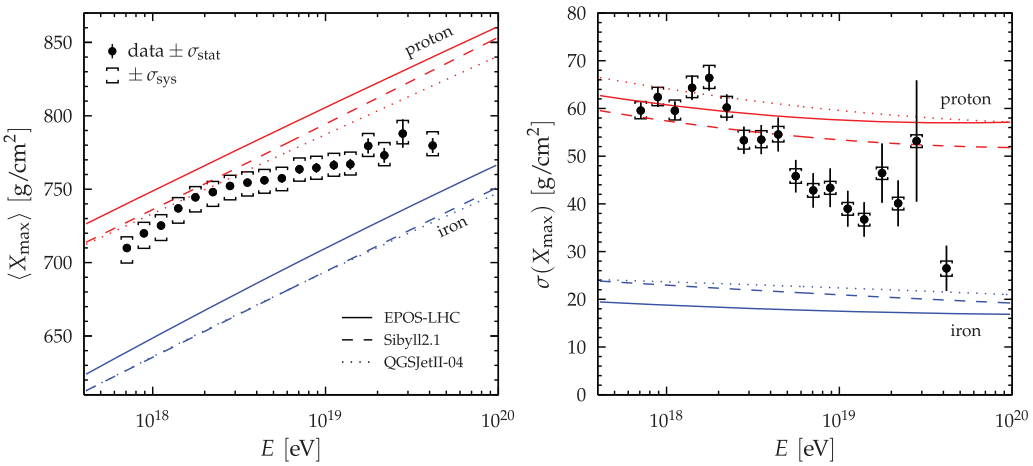

Fig. 1. – Energy evolution of the first two central moments of the $X_{\rm max}$ distribution compared to air-shower simulations for proton and iron primaries [14].

reaches its maximum, called $X_{\rm max}$, is a standard parameter used to extract composition information as different nuclei produce different distributions of $X_{\rm max}$ [10]. The first two moments of $X_{\rm max}$, the mean $\langle X_{\rm max} \rangle$ and dispersion $\sigma(X_{\rm max})$, have been used [11, 12] to infer information on the composition since the mean scales linearly with the logarithm of the primary mass $\ln A$.

Additionally, the Auger Collaboration has proposed different methods [13] to infer the composition that use the SD array, taking advantage of the large statistical sample provided by the increased duty cycle. These methods involve the measurement of observables related to muon content.

In this paper we summarise the latest results concerning the first two $X_{\rm max}$ moments as well as the results of fitting to the total $X_{\rm max}$ distributions. We also show the latest results of muon studies, involving the muon number in highly inclined events and the muon production depth distribution, which allow us to constrain the hadronic interaction models.

2. – Depth of the shower maximum

The Pierre Auger Collaboration has published studies of the mean and dispersion of the $X_{\rm max}$ distribution at energies above $10^{17.8}$ eV [14] as shown in fig. 1. Comparing the energy evolution of $X_{\rm max}$ for data and simulations it can be seen that the slope for the measurements is different from what would be expected for either pure proton or iron compositions. The evolution of $X_{\rm max}$ with the logarithm of energy is usually referred to as *elongation rate* [15-17]. A single linear fit does not describe the data well across the entire energy range (χ^2/ndf = 138.4/16), but allowing for a change in the elongation rate at a break point yields a good fit, with a χ^2/ndf of 8.2/14. This implies that there is a change in the evolution of the average composition of cosmic rays, tending towards lighter nuclei up to energies of $10^{18.3}$ eV then reversing and becoming heavier with increasing energy. A similar trend is visible for the width of the $X_{\rm max}$ distribution in the right panel of fig. 1.

For a more quantitative study of the evolution of the composition, $\langle X_{\rm max} \rangle$ and $\sigma(X_{\rm max})$ are converted to the first two moments of the $\ln A$ distribution, following the

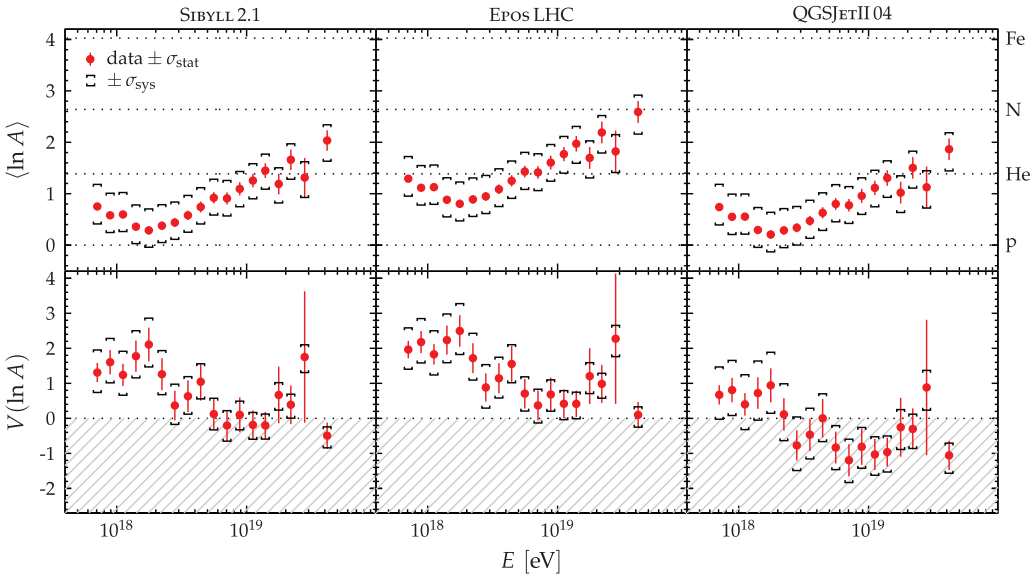

Fig. 2. – Average of the logarithmic mass and its variance estimated from data using different interaction models. The non-physical region of negative variance is indicated as the gray dashed region [14].

method described in [18, 19]. The mean and variance of $\ln A$ are shown in fig. 2 using simulations with three interaction models. In all three models it can be seen that the composition is the lightest at around $10^{18.3}$ eV. An interpretation using Epos-LHC leads to the heaviest average composition, followed by Sibyll2.1 and then QGSJetII-04. The variance of $\ln A$, derived with both Epos-LHC and Sibyll2.1, suggests a mixed composition at low energies which becomes dominated by a single composition about $10^{18.7}$ eV, where the variance is close to 0. The interpretation with QGSJetII-04 leads to variances less than 0 which are unphysical and therefore this model is disfavoured by the data.

Another approach is based on using the full $X_{\max}$ distributions. This approach maximises the information, reducing any possible degeneracies that can occur when one considers only the first two moments of the $X_{\max}$ distribution. For a given hadronic interaction model, the $X_{\max}$ distribution is compared to predictions made using Monte Carlo simulations formed with varying nuclear fractions, and a binned maximum-likelihood discriminator is used to choose the best-fit fractions [12].

The hybrid $X_{\max}$ dataset in the range $E = 10^{17.8}$ to 10^{20} eV, measured by Auger, was used to determine whether it can be described satisfactorily by an evolution of composition with energy. First a mixture of the two most stable types of particles, protons and iron nuclei, is considered and then the fits are extended to include extra components. Specifically, helium and nitrogen nuclei are included as representatives of the intermediate range of nuclear masses. The fit quality is measured by the p-value, which is defined as the probability of obtaining a worse fit (larger likelihood) than that obtained with the data.

The fit result for the mix of protons, helium, nitrogen and iron is shown in fig. 3. The two component fit gives poor quality agreement, indicating that none of the hadronic interaction models can describe the data as a simple mixture of protons and iron nuclei. Adding the intermediate components greatly improves the fits for all hadronic interaction

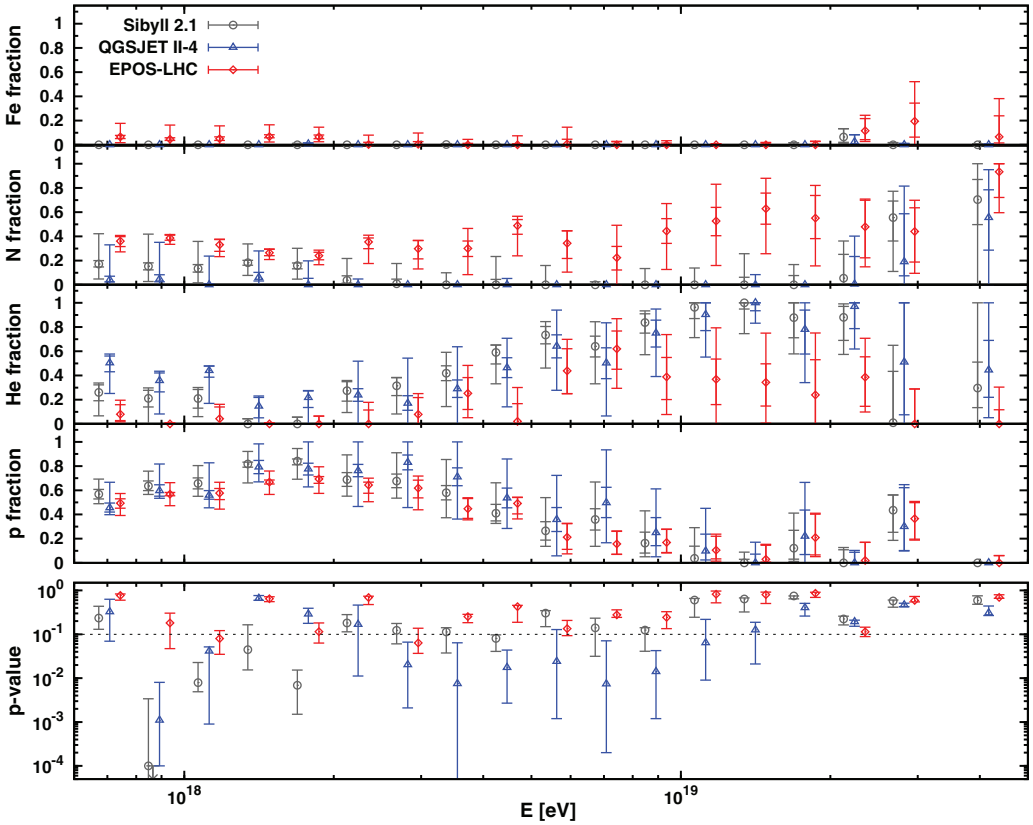

Fig. 3. – Fitted fraction and quality for the scenario of a complex mixture of protons, helium nuclei, nitrogen nuclei, and iron nuclei. The upper panels show the species fractions and the lower panel shows the p-values [12].

models, and a common feature appears to be very little need to include any iron primaries at all energies. In particular results using EPOS-LHC are satisfactory over most of the energy range. All three models considered give similar results for the evolution with energy of the proton fraction. However, it is still possible that the observed trend is due to deviations from the standard extrapolations in hadronic interaction models, rather than an evolution of the composition mix.

3. – Muons in air showers at the Pierre Auger Observatory

The number of muons in an air shower is another powerful indicator of the primary mass. Simulations show that the produced number of muons, N_μ, rises almost linearly with the cosmic-ray energy, and increases with a small power of the cosmic-ray mass. This behaviour can be understood in terms of the generalised Heitler model of hadronic air showers [20]. The muon number in inclined air showers is measured using a relative scale number called N_{19}. This value is defined as the relative measure of the observed muon densities at the ground to the average muon density profile of simulated proton air showers of fixed energy 10^{19} eV. This value is then corrected for the average bias, to get an unbiased estimator called R_μ [21].

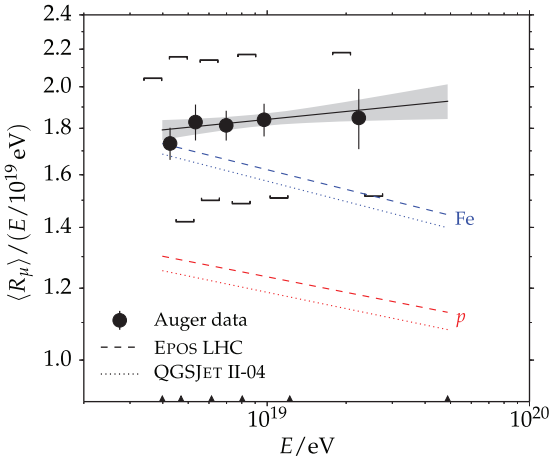

Fig. 4. – Average muon content $\langle R_\mu \rangle$ per shower energy E as a function of the shower energy E in double logarithmic scale. Data are shown bin-by-bin (circles) together with the fit (line) [21]. Square brackets indicate the systematic uncertainty of the measurement, while the diagonal offsets represent the correlated effect of systematic shifts in the energy scale. The grey band indicates the statistical uncertainty of the fitted line. Shown for comparison are theoretical curves for proton and iron showers simulated at $\theta = 67°$ (dotted and dashed lines, respectively). Black triangles at the bottom show the energy bin edges. The binning was adjusted by an algorithm to obtain equal numbers of events per bin.

The muon content R_μ of individual showers with the same arrival direction and energy varies. This is caused by statistical fluctuations in the development of the hadronic cascade, and, in addition, by random sampling from a possibly mixed mass composition. We refer to these as intrinsic fluctuations. In the following, we make statements about the average shower, meaning that the average is taken over these intrinsic fluctuations.

The resulting parameter $\langle R_\mu \rangle$ is shown in fig. 4, where square brackets indicate the systematic uncertainty of the measurement and the grey band indicates the statistical uncertainty of the fitted line. The ratio $\langle R_\mu \rangle / (E/10^{19}\,\mathrm{eV})$ cancels most of the energy scaling and emphasises the effect of the cosmic-ray mass on the muon number. The theoretical curves are shown for comparison for proton and iron showers simulated at 67°. These curves are well separated, which illustrates the power of $\langle R_\mu \rangle$ as a composition estimator. The measured muon number is higher than in pure iron showers, suggesting contributions from even heavier elements. This interpretation is not in agreement with the studies based on X_{max} shown above.

The other parameter presented comes from the reconstruction of the distribution of muon production depths (MPD). Since muons come from the decay of pions and kaons, the shape of the MPD distribution contains information about the evolution of the hadronic cascade. The point at which the production of muons reaches its maximum as the shower develops through the atmosphere is called X^{μ}_{max}. The muon production depth distribution is obtained using the arrival times of the muonic component at the ground [22], thanks to a set of simple assumptions. This evolution of the measured $\langle X^{\mu}_{\mathrm{max}} \rangle$ as a function of energy is illustrated in fig. 5. The data show a flatter trend than either pure proton or iron predictions. While the data are bracketed by QGSJETII-04, they fall below the EPOS-LHC estimates for iron.

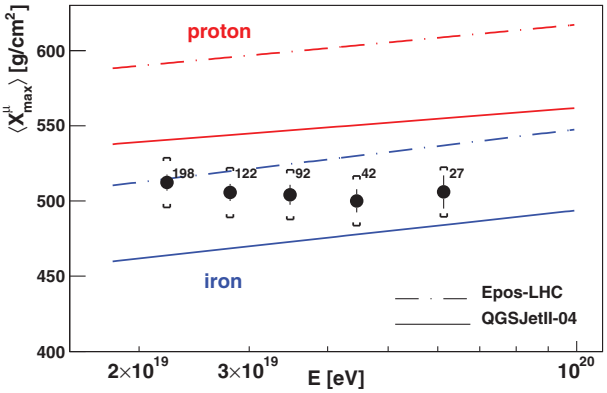

Fig. 5. – Measured $\langle X^{\mu}_{\rm max}\rangle$ as a function of energy. The predictions of different hadronic models for protons and iron are shown. Numbers indicate the number of events in each energy bin, and brackets represent the systematic uncertainty [22].

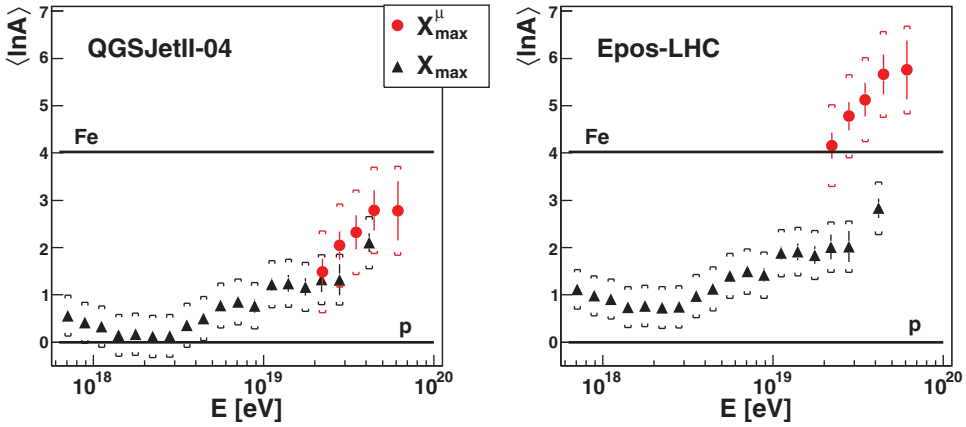

Fig. 6. – Conversion of $\langle X^{\mu}_{\rm max}\rangle$ (circles) and $\langle X_{\rm max}\rangle$ (triangles) [23] to $\langle \ln A\rangle$, as a function of energy. On the left (right) plot we use QGSJetII-04 (Epos-LHC) as the reference hadronic model. See text for a detailed discussion of the difference between models. Brackets correspond to the systematic uncertainties [22].

Figure 6 shows the conversion of the $\langle X^{\mu}_{\rm max}\rangle$, as well as the $\langle X_{\rm max}\rangle$, into $\langle \ln A\rangle$. For Epos-LHC the results indicate primaries heavier than iron at the highest energies. There is also an incompatibility between the $\langle \ln A\rangle$ values calculated from the $\langle X^{\mu}_{\rm max}\rangle$ and $\langle X_{\rm max}\rangle$ measurements. They are incompatible at a level of at least 2.5σ. With QGSJetII-04 we obtain compatible values, but this model has problems describing the first two moments of the $\ln A$ distribution calculated from the $X_{\rm max}$ measurements, shown above in fig. 2.

4. – Upgrade of the Observatory

The Pierre Auger Observatory has now been collecting data for over 10 years, 6 of which were with a fully instrumented array. While the results obtained so far have advanced our understanding, it is still not possible to determine whether the observed

Fig. 7. – Photo of a $4\,\mathrm{m}^2$ scintillation prototype detector placed on top of a water-Cherenkov detector. Not visible are additional $10\,\mathrm{m}^2$ scintillation detectors buried 1.3 m underground with power provided by the extra solar panel.

flux suppression is due to a maximum of energy in astrophysical sources, or due to the GZK-effect. This ambiguity must be resolved in order to identify sources. An event-by-event measurement of the composition of the cosmic rays will increase the quality of several analyses, including some of those outlined above.

The most promising method to obtain further composition sensitive information is to discriminate between the muonic and electromagnetic components of the shower by using ground array measurements. Intense R&D efforts have been ongoing and many different options of complementing the surface detector array have been investigated. The principle behind all these options is the same, using the different responses of two co-located detectors to extract the muonic and electromagnetic components.

A photo of a working prototype in the field is shown in fig. 7. It shows a $4\,\mathrm{m}^2$ scintillator, made of two units of $2\,\mathrm{m}^2$ each, read out by scintillating fibres which feed into PMTs. The signals are digitised by the current surface detector electronics, which will be replaced by new electronics, facilitating the readout of the extra channels and providing better monitoring and more powerful triggers. This detector design will undergo further optimisation.

This will also allow for a better understanding of the hadronic interactions at the highest energies. A smaller region of the array will also have scintillators buried underground (AMIGA detectors) in order to directly measure the muonic component of the showers.

5. – Conclusions and outlook

The parameters obtained with both the FD and SD detectors of the Pierre Auger Observatory demonstrate sensitivity in both mass composition information and in constraining hadronic interaction models. The latest measurements presented here continue to show a changing composition, with a trend towards heavier primaries with increasing energy. There is a deficit of muons in the hadronic models, shown by the discrepancies in the muon measurements. By improving the separation of the electromagnetic

and muonic shower component through an upgrade, the Pierre Auger Observatory will also improve the detection capabilities for high-energy photons and neutrinos and would enable stringent tests of hadronic interaction models at energies much higher than those available at the LHC.

* * *

The successful installation, commissioning, and operation of the Pierre Auger Observatory would not have been possible without the strong commitment and effort from the technical and administrative staff in Malargüe. We are very grateful to all the national agencies and organisations for financial support. The author thanks the organisers of the 29th Les Rencontres de Physique de la Vallée d'Aoste for the invitation to participate in this wonderful conference.

REFERENCES

[1] Abbasi R. U. *et al.* (HiRes Collaboration), *Phys. Rev. Lett.*, **100** (2008) 101101.
[2] Abraham J. *et al.* (Pierre Auger Collaboration), *Phys. Rev. Lett.*, **101** (2008) 061101.
[3] Abu-Zayyad T. *et al.* (TA Collaboration), *Astrophys. J.*, **768** (2013) L1.
[4] Abreu P. *et al.* (Pierre Auger Collaboration), *Astropart. Phys.*, **34** (2010) 314, [arXiv:1009.1855 [astro-ph.HE]].
[5] Aab A. *et al.* (Pierre Auger Collaboration), *Astrophys. J.*, **804** (2015) 15, [arXiv:1411.6111 [astro-ph.HE]].
[6] Abraham J. *et al.* (Pierre Auger Collaboration), *Nucl. Instrum. Methods A*, **523** (2004) 50.
[7] Aab A. *et al.* (Pierre Auger Collaboration), *Nucl. Instrum. Methods A*, **798** (2015) 172, [arXiv:1502.01323 [astro-ph.HE]].
[8] Allekotte I. *et al.* (Pierre Auger Collaboration), *Nucl. Instrum. Methods A*, **586** (2008) 409.
[9] Abraham J. *et al.* (Pierre Auger Collaboration), *Nucl. Instrum. Methods A*, **620** (2010) 227.
[10] Gaisser T. K. and Hillas A. M., *Proc. 15th ICRC, Plovdiv, Bulgaria*, **8** (1977) 353.
[11] Abraham J. *et al.* (Pierre Auger Collaboration), *Phys. Rev. Lett.*, **104** (2010) 091101, [arXiv:1002.0699 [astro-ph.HE]].
[12] Aab A. *et al.* (Pierre Auger Collaboration), *Phys. Rev. D*, **90** (2014) 122006.
[13] Garcia-Pinto D., for the Pierre Auger Collaboration, *Proc. 32nd ICRC, Beijing, China* (2011), doi:10.7529/ICRC2011/V02/0709 [arXiv:1107.4804 [astro-ph]].
[14] Aab A. *et al.* (Pierre Auger Collaboration), *Phys. Rev. D*, **90** (2014) 122005.
[15] Linsley J., *Proc. 15th ICRC, Plovdiv, Bulgaria*, **12** (1977) 89.
[16] Gaisser T. K., McComb T. J. K. and Turver K. E., *Proc. 16th ICRC, Kyoto, Japan*, **9** (1979) 258.
[17] Linsley J. and Watson A. A., *Phys. Rev. Lett.*, **46** (1981) 459.
[18] Abreu P. *et al.* (Pierre Auger Collaboration), *JCAP*, **1302** (2013) 026.
[19] Ahn E. J. *et al.* (Pierre Auger Collaboration), *Proc. 33rd ICRC, Rio de Janeiro, Brazil* (2013), [arXiv:1307.5059].
[20] Matthews J., *Astropart. Phys.*, **22** (2005) 387.
[21] Aab A. *et al.* (Pierre Auger Collaboration), *Phys. Rev. D*, **91** (2015) 032003.
[22] Aab A. *et al.* (Pierre Auger Collaboration), *Phys. Rev. D*, **90** (2014) 012012.
[23] Letessier-Selvon A. *et al.* (Pierre Auger Collaboration), *Braz. J. Phys.*, **44** (2014) 560.